PERGAMON

International Journal of Heat and Mass Transfer 45 (2002) 495–507

International Journal of HEAT and MASS TRANSFER

www.elsevier.com/locate/ijhmt

A model for high-pressure vaporization of droplets of complex liquid mixtures using continuous thermodynamics

Guang-Sheng Zhu [1], Rolf D. Reitz *

Engine Research Center, University of Wisconsin-Madison, 1011 Engineering Research Building, 1500 Engineering Drive, Madison, WI 53706, USA

Received 5 May 2000; received in revised form 9 May 2001

Abstract

This paper presents a comprehensive model for the transient high-pressure vaporization process of droplets of complex liquid mixtures with large number of components in which the mixture composition, the mixture properties, and the vapor–liquid equilibrium (VLE) are described by using the theory of continuous thermodynamics. Transport equations, which are general for the moments and independent of the distribution functions, are derived for the semi-continuous systems of both gas and liquid phases. A general treatment of the VLE is conducted which can be applied with any cubic equation of state (EOS). Relations for the properties of the continuous species are formulated. The model was further applied to calculate the sub- and super-critical vaporization processes of droplets of a representative petroleum fuel mixture – diesel fuel. The results show that the liquid mixture droplet exhibits an intrinsic transient vaporization behavior regardless of whether the pressure is sub- or super-critical. The regression rate of the liquid mixture droplet is reduced significantly during the late vaporization period. The comparison with the results of a single-component substitute fuel case emphasizes the importance of considering the multi-component nature of practical mixture fuel and the critical vaporization effects in practical applications. This paper provides a practical means for more realistically describing the high-pressure vaporization processes of practical fuels.

1. Introduction

Droplet vaporization has been the focus of numerous studies for decades due to both its theoretical and practical significance. In most engineering applications the vaporization process takes place in high-pressure environments. The liquids employed, such as petroleum fuels in internal combustion engines, are a complex mixture which is typically composed of hundreds of components. This complex mixture exerts a significant effect on the vaporization process which, as shown by Sirignano and Law [1], cannot be readily described by a single-component fuel substitute.

Several investigations have been conducted on droplet high-pressure vaporization, as reviewed by Givler and Abraham [2]. More recent studies include the works of Stengele et al. [3], Curtis et al. [4], Zhu and Aggarwal [5,6], and Abraham and Givler [7]. Most of this work has concentrated on the vaporization of single-component liquid droplets. Very little work appears in the literature on liquid mixtures with more than one component, and typical studies include the calculations of Lazar and Faeth [8] using quasi-steady models, and those of Stengele et al. [3] and Hsieh et al. [9] using unsteady models. In these studies the liquid mixture was represented by just two components with distinctly different boiling temperatures. The methods are developed for treating a small number of discrete components. However, it is very difficult or practically impossible to apply these methods to practical fuels based on the fact that either the number of components is too large to be numerically accounted for or there is no way to isolate and identify the different chemical species.

* Corresponding author. Tel.: +1-608-262-0145; fax: +1-608-262-6707.

E-mail addresses: zhugs@erc.wisc.edu (G.-S. Zhu), reitz@engr.wisc.edu (R.D. Reitz).

[1] Tel.: +1-608-265-6432; fax: +1-608-262-6707.

0017-9310/02/$ - see front matter
PII: S0017-9310(01)00173-9

Therefore, there are generally no models available to consider the high-pressure vaporization of droplets of complex liquid mixtures with large numbers of components.

An alternative approach to treat complex liquid mixtures is to employ the thermodynamics of continuous systems, in which the liquid composition, and consequently the system properties, are represented and described by continuous probability density functions. This idea of treating complex mixtures has been mostly applied in chemical engineering. Only recently has it been applied to the field of droplet evaporation in low-pressure environments by Tamim and Hallett [10], and to the field of spray combustion by Lippert and Reitz [11]. The latter one also employed a low-pressure quasi-steady vaporization model for its practical applicability in multi-dimensional engine simulations.

In this paper a comprehensive new model is developed for vaporizing droplets with large numbers of components in high-pressure environments. The transport equations for both gas and liquid phases, together with a general treatment for the vapor–liquid equilibrium (VLE), are derived and solved. Relations for the properties of the high-pressure sub- and supercritical vaporization processes are formulated. Finally, typical results for a representative petroleum fuel – diesel fuel – along with the results for a single-component fuel for comparison are presented and analyzed.

2. Theoretical formulation

The physical model considers a fuel droplet of complex liquid mixtures with large numbers of components vaporizing in a non-convective high-pressure gas environment. Radiation and second-order effects such as the Soret and Dufour effects are assumed to be negligible. A spherically symmetric vaporization process is assumed. The fuel composition in continuous thermodynamics is represented by molar distribution functions $f^l(\tau)$ and $f^v(\tau)$ for the liquid and vapor phases, respectively. The ambient gas is treated as discrete species. Thus the formulation considered here deals with two semi-continuous mixture systems, e.g., the system of liquid phase including liquid fuel (continuous) and the dissolved ambient gas (discrete) and the system of gas-phase including the fuel vapor (continuous) and the gas ambience (discrete). The general molar distribution function for the composition of each semi-continuous system is defined as:

$$G^p(\tau) = y_f^p f^p(\tau) + \sum_{s=1}^{N} y_s^p\, \delta(\tau - \tau_s), \tag{1}$$

$$\int_0^\infty G^p(\tau)\, \mathrm{d}\tau = 1,$$

$$\int_0^\infty f^p(\tau)\, \mathrm{d}\tau = 1, \tag{2}$$

$$\sum_{s=1}^{N} y_s^p = 1 - y_f^p,$$

where the superscript p represents v or l, denoting the properties of the vapor or liquid phases, respectively. y is the mole fraction, N the total number of discrete species, and δ the Dirac delta function. Subscripts s and f, respectively, denote the properties of discrete and fuel species. The independent variable τ is some characterizing property that is chosen to be molecular weight in this paper. The molar distribution function $f(\tau)$ is only applicable for the continuous species. With the use of both continuous thermodynamics theory [12] for the continuous fuel species and the conventional theory [6] for the discrete species, we derive in the following the transient governing equations for both the gas and liquid-phase semi-continuous systems, along with the inter-phase conditions at the droplet surface.

2.1. Governing equations for gas-phase

The governing equations for the continuity of discrete species and for the momentum of the gas-phase system have the same forms as those in [6]. For the continuous species, the governing equation for the moments of the distribution is written as

$$\frac{\partial}{\partial t}[\rho_f (\theta^n)^v] + \nabla \cdot [\rho_f (\theta^n)^v u] = -\nabla \cdot \int_0^\infty \tau^n J_\tau\, \mathrm{d}\tau \quad (n = 0, 1, 2, \ldots), \tag{3}$$

where u and ρ_f are the velocity of the gas-phase mixture and the density of the fuel vapor, respectively. J_τ is the molar diffusion flux for the element with molecular weight τ, and in this study Fick's law is assumed applicable for the semi-continuous system. θ^n represents the nth moment about the origin of the distribution and is defined as

$$(\theta^n)^p = \int_0^\infty \tau^n f^p(\tau)\, \mathrm{d}\tau \quad (n = 0, 1, 2, \ldots). \tag{4}$$

Any number of equations can be obtained with Eq. (3) with different values of n, but for a two-parameter type distribution function that is typically selected for petroleum fuels, $n = 2$ will suffice for calculations by describing the variation of the fuel vapor composition in space and time through the equation for vapor mole fraction ($n = 0$), and the equations for the first and the second moments of the distribution ($n = 1$ and 2, respectively) (see Appendix A).

The energy equation for the gas phase semi-continuous system is derived as

$$\frac{\partial}{\partial t}(\rho I) + \nabla\cdot(\rho u I) + P\nabla\cdot u = -\nabla\cdot\left[k\nabla T + \sum_{s=1}^{N} h_s(T)J_s + \int_0^\infty h_f(\tau,T)J_\tau\right] - \Pi\cdot\nabla u, \quad (5)$$

where P, T and ρ are the pressure, the temperature and the density of the gas phase system, respectively. Π is the viscous stress tensor, k is the thermal conductivity and J_s is the molar flux of the sth discrete species. I is the specific internal energy of the gas phase mixture, which is related to the pressure and temperature by

$$I = \left[\sum_{s=1}^{N}\frac{\rho_s}{\rho}h_s(T) + \int_0^\infty f^v(\tau)h_f(\tau,T)\,\mathrm{d}\tau\right] - \frac{P}{\rho}, \quad (6)$$

where $h_s(T)$ and $h(\tau,T)$ are the enthalpies of the sth discrete species and the continuous species with molecular weight τ, respectively, which are obtained from JANAF tables for the discrete species and from empirical formulations for the continuous species as described in Appendix A.

A cubic equation of state (EOS) is employed for the semi-continuous system and the subsequent VLE calculation, which can be written in a general form as [14]

$$P = \frac{RT}{V-b} - \frac{a}{V^2+qbV+wb^2}, \quad (7)$$

where V is the volume of a semi-continuous system and R is the universal gas constant. q and w are constants depending on the type of cubic EOS. Their values are: $q=2$, $w=1$ for the Peng–Robinson EOS (PR-EOS), and $q=1$, $w=0$ for the Soave–Redlich–Kwong (SRK-EOS) and the Redlich–Kwong EOS (RK-EOS). Parameters a and b are functions of temperature and species mole fractions obtained via mixing rules with their corresponding values for each discrete species and the continuous one (see Appendix B). For discrete species, the expressions of the corresponding cubic EOS are directly employed for calculating the values of these parameters. For continuous fuel species, a set of empirical formulae is derived. They are formulated for n-alkanes from c_2 to c_{20} for temperatures from 270 to 1500 K as follows:

$$a^{0.5}(\tau,\tau) = a_0(T) + a_1(T)\tau,$$
$$a_0(T) = a_{00} + a_{01}T + a_{02}T^2, \quad (8)$$
$$a_1(T) = a_{10} + a_{11}T + a_{12}T^2,$$
$$b(\tau) = b_0 + b_1\tau. \quad (9)$$

Table 1 gives all the coefficients for the specified range of temperatures and molecular weights. It was shown [6] that PR- and SRK-EOS are superior to RK-EOS in both VLE and droplet vaporization calculations. Table 1 illustrates all the coefficients for both PR- and SRK-EOS. These formulae have been compared with the expressions from corresponding cubic EOS for these constants. It was found that the relative errors of these formulae are generally less than 5%.

2.2. Governing equations for liquid phase

The forms of the governing equations used for the liquid phase directly relate to the model employed to describe the droplet interior flow. The real case for a vaporizing droplet generally lies somewhat in between the well-mixed and the diffusion-limit cases [15]. The departures from the well-mixed state are more pronounced for multi-component mixtures with vastly different boiling points and for high-pressure conditions due to gas absorption. However, the effects of the departures are of less importance for mixtures with closely spaced component boiling points, and further, the effects on the total fuel concentration are even much less, as indicated by Tamim and Hallett [10]. Studies of high-pressure evaporation have also shown that the gas absorption is limited to a thin outer layer of the vaporizing droplet throughout the droplet lifetime [2,5,6]. With these considerations, the droplet interior is approximated with a two-zone model, in which the dissolved gas is assumed to exist only in the outer layer of the droplet and all other liquid properties are assumed as well mixed. Similar models have been employed by other researchers [4,16].

Suppose the ratio of the volume of the gas-absorbed layer to the total droplet volume is v_a. With the above

Table 1
Constants for PR- and SRK-EOS parameters for alkane fuels c_2–c_{20}

	a (bar cm^6/mol^2)				b (cm^3/mol)	
		a_{*0}	a_{*1}	a_{*2}		
PR-EOS	a_0	-1.8050×10^2	7.9164×10^{-1}	-1.5841×10^{-4}	b_0	-2.8946×10^1
	a_1	8.9542×10^1	-6.9257×10^{-2}	1.3855×10^{-5}	b_1	1.6248
SRK-EOS	a_0	-3.5926×10^2	7.6707×10^1	-1.6114×10^{-4}	b_0	-3.1734×10^1
	a_1	9.3905×10^1	-7.8067×10^{-2}	1.6399×10^{-5}	b_1	1.8094

assumptions, the fuel molar flux from the droplet surface is derived as

$$\dot{m}_f = \frac{1}{A}\frac{\mathrm{d}}{\mathrm{d}t}\left\{\int_0^\infty f^l(\tau)V_l c_l[v_a x_f + (1-v_a)]\,\mathrm{d}\tau\right\}, \tag{10}$$

where A and V_l are the surface area and the volume of the droplet, respectively. c_l is the molar density and x the molar fraction in the liquid-phase. Based on the mass balance at the droplet surface and using Eq. (10), the governing equations for the liquid-phase semi-continuous system can be derived as

$$x_{\mathrm{feq}}\frac{c_l r_s}{3}\frac{\mathrm{d}(\theta^n)^l}{\mathrm{d}t} - \left(x_{\mathrm{feq}}\dot{m} - v_a\frac{c_l r_s}{3}\frac{\mathrm{d}x_f}{\mathrm{d}t}\right)(\theta^n)^l = \left[\int_0^\infty \tau^n J_\tau\,\mathrm{d}\tau - y_f(\theta^n)^v\right]\Big|_{r_s^+} \quad (n=0,1,2,\ldots), \tag{11}$$

where r_s is the droplet radius. $(\theta^n)^l$ and $(\theta^n)^v$ are the nth moments of the distributions of the liquid fuel and its vapor, respectively, as defined in Eq. (4). The equivalent molar fraction of the liquid-phase x_{feq} is defined as

$$x_{\mathrm{feq}} = v_a x_f + (1-v_a). \tag{12}$$

Again, similar to Eq. (3) of the gas phase, here any number of equations can be obtained with Eq. (11) with different values of n. However, for a two-parameter type distribution $n=2$ suffices for calculations by describing the variation of the liquid composition with time through the vaporization molar flux, and the first and the second moments of the liquid distribution (see Appendix A). Zero and unity values of v_a correspond to no gas absorption and infinite diffusion coefficient conditions, respectively. However, the present calculations showed that v_a has little effect on the droplet vaporization behavior except for a slight influence on the results of the liquid fuel composition.

2.3. Boundary conditions and VLE

Far from the droplet, the temperature and pressure are set to be the corresponding ambient values, and the fuel vapor density and its product with the nth moment of the vapor distribution function are set to be zero. At the droplet surface, the boundary conditions are expressed using mass conservation (Eq. (11) with $n=0$), the energy equation (13) and thermodynamic equilibrium represented by Eq. (14)

$$\frac{r_s}{3}\rho_l c_{pl}\frac{\partial T_l}{\partial t} = k_l\nabla T|_{r_s^+} + \sum_{s=1}^{N} J_s\Delta H_s|_{r_s} + \int_0^\infty J_\tau\Delta H_\tau|_{r_s}, \tag{13}$$

$$G^v(\tau)\varphi^v(\tau) = G^l(\tau)\varphi^l(\tau), \tag{14}$$

where ΔH is the enthalpy of vaporization obtained via a VLE calculation as described later. c_p is the specific heat of constant pressure. Subscript l denotes the properties of the liquid-phase.

Eq. (14) expresses the VLE at the droplet surface. At low pressures where an ideal gas and ideal solution can be assumed, the equilibrium is normally expressed by Raoult's law. At elevated pressures, however, only the more general thermodynamic formulation of Eq. (14) is justified. For the semi-continuous system considered here, the fugacity coefficients φ^v for the gas phase and those for the liquid-phase φ^l are given by the following general chemical potential relation:

$$\mu(\tau) = \int\left\{\left[\frac{\delta P}{\delta n G(\tau^+)}\right]_{T,V,\tau^+=\tau} - \frac{RT}{V}\right\}\mathrm{d}V - RT\left[\frac{P^0 V}{nG(\tau)RT}\right] + RT + \mu^0(T,\tau), \tag{15}$$

where n is the total number of moles of substance. μ^0 is the ideal gas chemical potential at temperature T and reference pressure P^0. By substituting the general form of the cubic EOS Eq. (7) into Eq. (15), the corresponding formula for the fugacity coefficient for the semi-continuous system is derived as

$$\ln\varphi^\zeta = \frac{b(\zeta)}{b}(z-1) - \ln(z-B^*) + A_{\mathrm{eos}}\left(\frac{b(\zeta)}{b} - C_\zeta\right), \tag{16}$$

where

$$A_{\mathrm{eos}} = \frac{A^*}{B^*\sqrt{q^2-4w}}\ln\frac{2z+B^*(q+\sqrt{q^2-4w})}{2z+B^*(q-\sqrt{q^2-4w})},$$

$$A^* = \frac{aP}{R^2T^2}, \quad B^* = \frac{bP}{RT}$$

and z is the compressibility factor. For discrete species, $\zeta = s$ and

$$C_s = \frac{2}{a}\left[\sum_{j=1}^{N} y_j a(s,j) + y_f\int_0^\infty f(\tau)a(s,\tau)\,\mathrm{d}\tau\right]. \tag{16a}$$

For continuous species, $\zeta = \tau$ and

$$C_\tau = \frac{2}{a}\left[\sum_{j=1}^{N} y_j a(\tau,j) + y_f\int_0^\infty f(\tau)a(\tau,\tau)\,\mathrm{d}\tau\right]. \tag{16b}$$

The quantities a with double subscripts are the cross terms calculated via the mixing rule (see Appendix B). With Eq. (16) and the formulae for EOS parameters a and b given in Eqs. (8) and (9), the fugacity coefficients in the vapor-phase for the continuous fractions can further be expressed as an explicit function of molecular weight

$$\ln\varphi^v(\tau) = C_k^{(1)} + C_k^{(2)}\tau, \tag{17}$$

Table 2
Constants for calculating critical properties and boiling temperature for alkane fuels c_2–c_{20}

	Critical pressure (bar)	Critical temperature (K)	Boiling temperature (K)
χ_0	5.5590×10^1	2.2636×10^2	1.1166×10^2
χ_1	-3.3177×10^{-1}	3.6471×10^0	2.9582×10^0
χ_2	6.3261×10^{-4}	-6.3057×10^{-3}	-4.2393×10^{-3}

where the coefficients $C_k^{(1)}$ and $C_k^{(2)}$ are derived as:

$$C_k^{(1)} = \frac{b_0}{b}(z-1) - \ln(z-B^*) + A_{\text{eos}}\left\{\frac{b_0}{b} - \frac{2a_0}{a}\left[\sum_{j=1}^{N} y_j a^{0.5}(j,j)(1-k_{\tau j}) + y_f(a_0 + a_1\theta)\right]\right\}, \tag{17a}$$

$$C_k^{(2)} = \frac{b_1}{b}(z-1) + A_{\text{eos}}\left\{\frac{b_1}{b} - \frac{2a_1}{a}\left[\sum_{j=1}^{N} y_j a^{0.5}(j,j)(1-k_{\tau j}) + y_f(a_0 + a_1\theta)\right]\right\}, \tag{17b}$$

where the quantity $k_{\tau j}$ is the interaction coefficient between the discrete and the continuous species. Since there is no such kind of data available in reference for diesel fuel system, this quantity is taken to be zero in the calculations of the following section. The same formula as Eq. (17) holds for the fugacity coefficient of the liquid-phase of continuous species, with the properties of liquid phase replacing the corresponding properties in Eqs. (17a) and (17b). It is worth noting that the equations derived above are general for cubic type EOS. Therefore, any type of cubic EOS covered by Eq. (7) can conveniently be used for VLE and/or vaporization process calculations using the above equations. In this work the PR-EOS was selected for both the VLE and the vaporization process calculations.

For a mixture system, the heat of vaporization of each species is defined as the difference between the partial molar enthalpy of this species in the vapor- and liquid-phases. The following thermodynamic relation gives the partial molar enthalpy for both the discrete and continuous species:

$$\bar{H}_\zeta - \bar{H}_\zeta^0 = RT^2 \frac{\partial}{\partial T}(\ln \varphi^\zeta), \tag{18}$$

where the superscript 0 denotes the quantity in its ideal state.

2.4. Thermophysical properties

The thermodynamic and transport properties are considered to be functions of pressure, temperature and composition. For the discrete species, the diffusivity is calculated by means of the Chapman–Enskog theory in conjunction with the collision integrals given in [14]. For the continuous species, the formulae in [10] were employed for the diffusivities of the vapor, the first and the second moments of the composition. All the diffusivities were then corrected for pressure effects by using the Takahashi correlation [14]. The critical and boiling properties for the continuous species are formulated for n-alkanes from c_2 to c_{20} with the following form:

$$\chi = \chi_0 + \chi_1\tau + \chi_2\tau^2. \tag{19}$$

Table 2 gives all the constants for the specified range of molecular weights. It was found that the relative errors of these formulae are generally less than 3% as compared to the data of [14]. A generalized thermodynamic correlation based on a three-parameter corresponding state [18] was used to calculate the enthalpy correction for high-pressure effects for both discrete and continuous species. The method reported by Chung [17] was employed to calculate the thermal conductivity and viscosity of the gas phase at high pressures. The liquid density was directly calculated by the PR-EOS.

An arbitrary Lagrangian–Eulerian numerical method with adaptive mesh [6] was employed to solve the equations for the gas phase system. The equations for the liquid-phase system were solved using Runge–Kutta method. The solutions for both systems are coupled with each other through the regressing droplet surface conditions.

3. Results and discussion

The model derived in the above section is independent of the form of the distribution function that is selected for the continuous fuel species. In the present work, the Γ distribution, which is of a two-parameter type and often used to represent petroleum fractions [10,11], was chosen for the distributions of both vapor and liquid phases such that

$$f(\tau) = \frac{(\tau-\gamma)^{\alpha-1}}{\beta^\alpha \Gamma(\alpha)} \exp\left[-\frac{(\tau-\gamma)}{\beta}\right], \tag{20}$$

where γ is the origin, α and β are parameters controlling the shape, and $\Gamma(\alpha)$ is the gamma function, with the mean molecular weight $\theta = \alpha\beta + \gamma$ and variance $\sigma^2 = \alpha\beta^2$. A typical commercial petroleum fuel – diesel was chosen to be the liquid mixture studied. The composition parameters of this fuel are: $\alpha_L = 18.5$, $\beta_L = 10.0$ and $\gamma_L = 0.0$, with $\theta_L = 185$ and $\sigma_L = 43$. These parameters are chosen so that the calculated distillation curves with the distribution reproduce best the corresponding ASTM D-86 experimental data [10]. For comparison, a single-component substitute fuel was also represented by setting for it a very narrow distribution with $\alpha_L = 100.0$, $\beta_L = 0.1$ and $\gamma_L = 175.0$, a species very close to *n*-tridecane. This single-component fuel has the same molecular weight as the mean molecular weight of diesel fuel, and thus the difference between the results for both fuel cases actually represents the effect of composition.

Calculations were first carried out for the VLE of a system containing liquid fuel and nitrogen. Fig. 1(a) shows the predicted phase-equilibrium concentrations versus temperature at four different reduced pressures of 0.5, 1, 3, and 10, where the solid curves represent the results for the diesel fuel–nitrogen system and the dashed ones for the single-component substitute fuel–nitrogen system. P_r represents the reduced pressure of the diesel fuel. (The critical pressure used here for P_r is determined to be 18.6 atm by Eq. (19). This reference pressure is also used for the single-component substitute fuel.) As seen in the figure, the results of both diesel and its substitute systems generally show similar characteristics, e.g., with increasing pressures, the critical mixing temperature and the fuel vapor mole fraction decrease, and the gas absorption in liquid-phase increases and becomes significantly large in the super-critical regime. However, the substitute fuel case shows a higher boiling temperature, a lower critical mixing temperature, and a significantly smaller vapor mole fraction over the whole sub-critical pressure range and in the super-critical pressure range beyond the vicinity of the critical mixing point, than those of diesel fuel case. These differences imply that, for droplet vaporization process, the single-component substitute fuel may reach mixing critical state earlier and produce a significantly different vaporization rate from that of real diesel fuel.

Fig. 1(b) presents the change in the composition of the fuel vapor corresponding to the diesel cases of $P_r = 10$ and 0.5 in Fig. 1(a). For a given pressure, both the mean molecular weight of the vapor and the width of the vapor distribution, represented by the variance, increase with increasing temperature. These indicate that with increasing temperature, the portion of heavy species in fuel vapor increases and the heavy end of the vapor distribution is continuously extended. For a certain temperature, the portion of heavy species in the vapor also increases with pressure, implying that the heavy species are more easily vaporized in higher pressure environments. At the critical mixing state, the vapor composition parameters become identical to those of the liquid mixture.

Fig. 2 further presents the heat of vaporization versus temperature for the three different reduced pressures of 1, 3, and 10. The solid lines are also for diesel–nitrogen system and the dashed lines for the single-component substitute fuel–nitrogen system. The heat of vaporization is a function of pressure, temperature, and the composition of liquid mixture rather than depends only on temperature as treated in low-pressure approximation. As seen in the figure, it decreases significantly with increasing pressure. When the pressure is high enough,

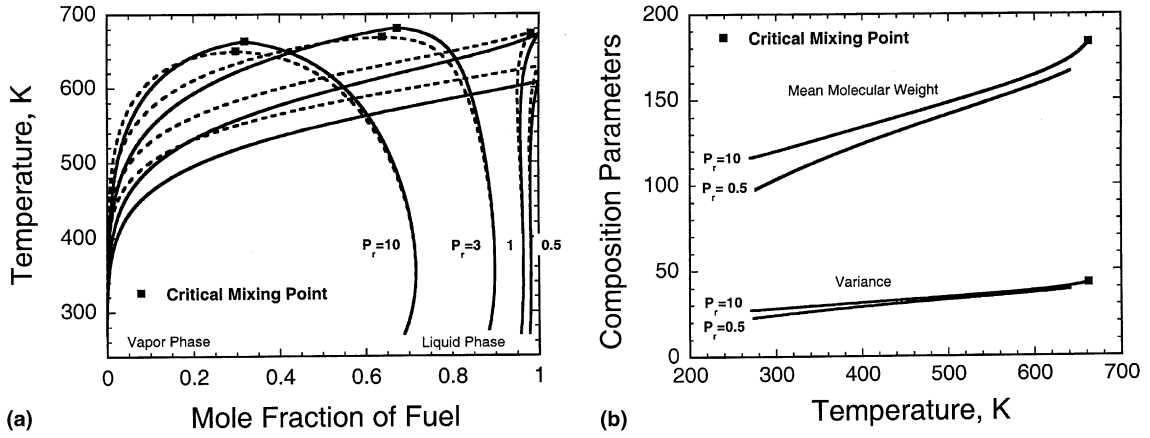

Fig. 1. (a) Fuel VLE concentrations versus temperature at four different reduced pressures of 0.1, 1.0, 3.0, and 10.0. $P_r = P/P_{crit}$ ($P_{crit} = 18.6$ atm). (b) Mean and variance of molecular weight of diesel fuel vapor under VLE versus temperature at two different reduced pressures of 0.5 and 10.0. Solid lines: diesel fuel with initial distribution parameters $\alpha = 18.5$, $\beta = 10.0$, and $\gamma = 0.0$. Dashed lines: single-component substitute fuel with $\alpha = 100.0$, $\beta = 0.1$, and $\gamma = 175.0$.

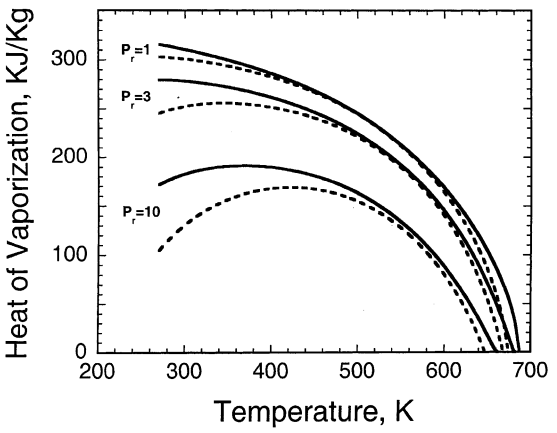

Fig. 2. Heat of vaporization versus temperature at three different reduced pressures of 1.0, 3.0, and 10.0. Solid lines: diesel fuel. Dashed lines: single-component substitute fuel.

the heat of vaporization increases, reaches a maximum value, and then decreases with increasing temperature. If the pressure is low, the heat of vaporization monotonously decreases with increasing temperature. As the system approaches its critical mixing state, the heat of vaporization drops rapidly to zero. The single-component substitute fuel case predicts a smaller heat of vaporization especially at low-temperature and high-pressure conditions. Since the substitute case system has a smaller critical mixing temperature (see Fig. 1(a)), it predicts the heat of vaporization that drops to zero at smaller temperatures.

We now focus on the transient vaporization processes of droplets of both the diesel fuel and its single-component substitute. The droplets considered are 0.1 mm in diameter and 300 K in temperature initially and are suddenly put into a nitrogen environment at 1500 K and at different pressures ranging from sub-critical to super-critical values of the diesel fuel. Fig. 3(a) presents the normalized surface temperatures versus time at four different reduced pressures of 0.1, 1, 3 and 5 for diesel fuel droplet (solid lines) and its single-component substitute fuel droplet (dashed lines). As seen from the figure, an obvious difference between the normalized surface temperatures of both droplets is that the temperature of the liquid mixture droplet is entirely transient no matter whether the pressure is sub-critical or super-critical.

The droplet surface temperature is actually determined by the heat flux H_e transferred from the environment, the energy flux H_c consumed for vaporizing the droplet, and the heat flux H_i transferred to droplet interior. H_i is generally about two orders of magnitude less than H_e for most of the droplet lifetime [6], and is hence less important to the surface temperature behavior. (For the well-mixed droplet vaporization model, $H_i = 0$. Here the analyses also include H_i for completeness.) The net value $H_e - H_c - H_i$ drives the surface temperature gradient with respect to time. In the sub-critical pressure regime, $H_e - H_c - H_i = 0$ will eventually be satisfied for a single-component fuel droplet, and it then behaves as a steady vaporization process at the pseudo wet-bulb temperature. However, for a liquid mixture droplet, H_e will always be larger than $H_c + H_i$ due to the continuously increasing droplet boiling temperature. This is seen in Fig. 4, where both the variation in droplet boiling temperature, T_b at $P_r = 0.1$ and the critical mixing temperature, T_c at $P_r = 3.0$ are presented.

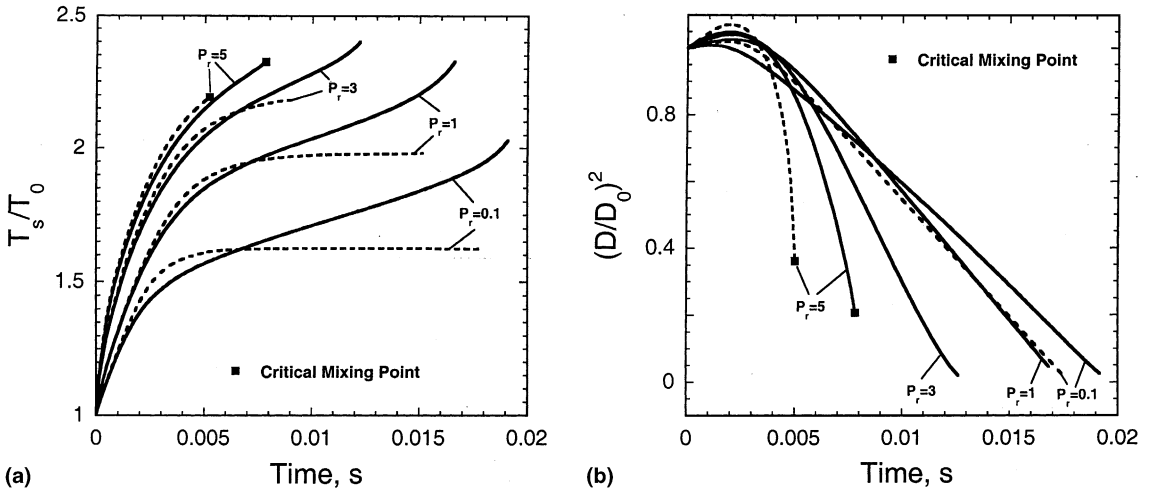

Fig. 3. (a) Normalized surface temperatures of droplets versus time and (b) normalized surface area of droplets versus time, at four different reduced pressures of 0.1, 1.0, 3.0, and 5.0, respectively. Solid lines: diesel fuel with initial distribution parameters $\alpha = 18.5$, $\beta = 10.0$, and $\gamma = 0.0$. Dashed lines: single-component substitute fuel with $\alpha = 100.0$, $\beta = 0.1$, and $\gamma = 175.0$.

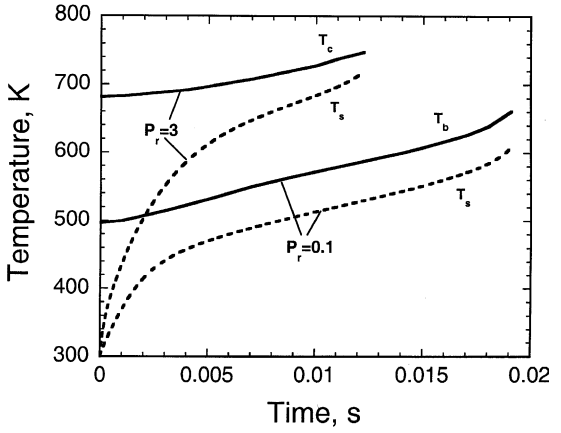

Fig. 4. Time histories of boiling temperature T_b at reduced pressure of 0.1 and critical mixing temperature T_c at reduced pressure of 3.0 for diesel droplet. T_s: Droplet surface temperature.

As the evaporation process proceeds, the lighter species are continuously preferably distilled, and the heavy species become more and more dominant in the composition (see also in Fig. 6). As seen from Fig. 4, the boiling and critical mixing temperatures increase continuously. The former increases almost at the same rate as that of the increase in droplet surface temperature (T_s in Fig. 4). Therefore, the heat-up process spans the whole droplet lifetime, and the droplet never reaches the boiling (web-bulb) state. At super-critical pressure, H_e is always larger than $H_c + H_i$ for droplets of both kinds of fuels. However, since only heavy components remain in the fuel mixture case during the later period of vaporization, it evaporates at a smaller rate and thus has a smaller value of H_c during this period than for the single-component fuel case. Consequently, its surface temperature increases even more sharply near the end of its lifetime, thus exhibiting a stronger transient behavior than that of the single-component fuel. Due to the continuous increase in critical mixing temperature and the lower volatility of the fuel, the fuel mixture droplet reaches its critical mixing state at a relatively high pressure of $P_r = 5$, while its single-component partner gains its critical mixing state much earlier.

Fig. 3(b) shows the normalized surface area of the diesel fuel droplet versus time for the same ambient cases as those of Fig. 3(a) (solid lines), together with the results for the single-component substitute fuel at two pressures of $P_r = 0.1$ and $P_r = 5$ (dashed lines). For the high ambient temperature case considered here, the droplet surface regression rate increases progressively with pressure, mainly as a result of the reduced heat of vaporization. The remaining heavy components in the fuel mixture cause the regression rate to decrease near the end of its lifetime (e.g., see $P_r = 3$ case). Another interesting behavior on these curves is that volumetric dilation occurs during the initial period of vaporization. The change of volume (or radius) is mainly determined by the vaporization rate and the change of liquid density. The initial rapid temperature rise and the gas absorption into the liquid-phase lead to a rapid decrease in liquid density and thus to an increase in droplet volume. On the other hand, the initial temperature rise also tends to enhance the droplet vaporization process and thus to reduce the volume. The extent of the volumetric dilation is actually the competing result of the above factors, and is closely related to the liquid volatility and/or the environmental pressure. For vaporizing conditions of less volatile fuels and/or higher pressure environments, the initial volumetric dilation is more obvious. The fuel considered here has a low volatility. As will be seen later, the initial vaporization rate is very small. Therefore, the initial change in the liquid density dominates the obvious volumetric dilation. The above vaporization behaviors are supported very well by experimental data [19], where an obvious reduced regression rate in the late vaporization period and an obvious initial volumetric dilation were measured for kerosene, a mixture whose volatility is close to that of the diesel fuel considered here.

Fig. 5 presents the vaporization rate and the fuel vapor mole fraction at the droplet surface for the $P_r = 3$ case. Compared to the single-component case, diesel fuel has a larger vapor mole fraction at the initial stage due to the lighter components distilling off first, and a smaller one at the later stages due to the heavier component remaining in liquid-phase. Consequently, the vaporization rate of the diesel fuel droplet is initially larger and becomes smaller sooner. It is seen that the vaporization rates of both fuels are extremely small, especially at the beginning of the process which, as

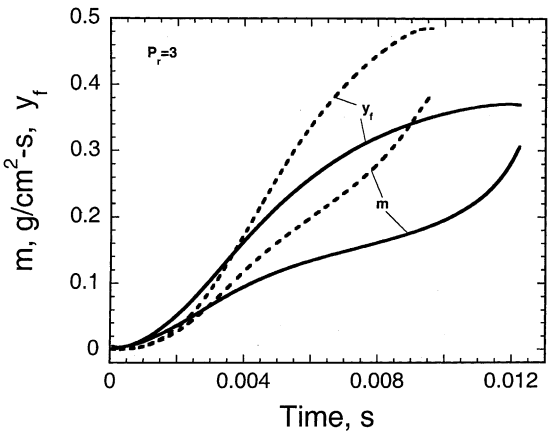

Fig. 5. Mass vaporization rate and vapor mass fraction at the droplet surface versus time at reduced pressure 3.0. Solid lines: diesel fuel. Dashed lines: single-component substitute fuel.

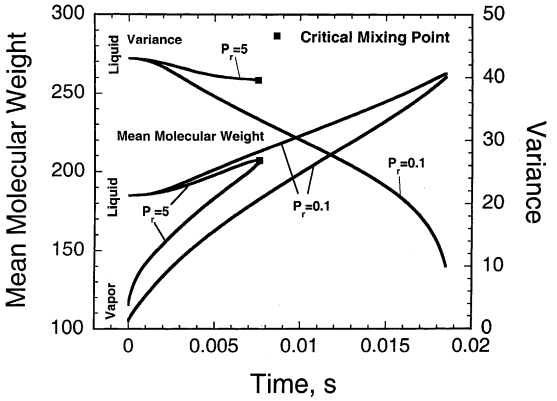

Fig. 6. Mean molecular weight of diesel droplet and its vapor at the droplet surface and the variance of the liquid phase distribution versus time at two different reduced pressures of 0.1 and 5.0.

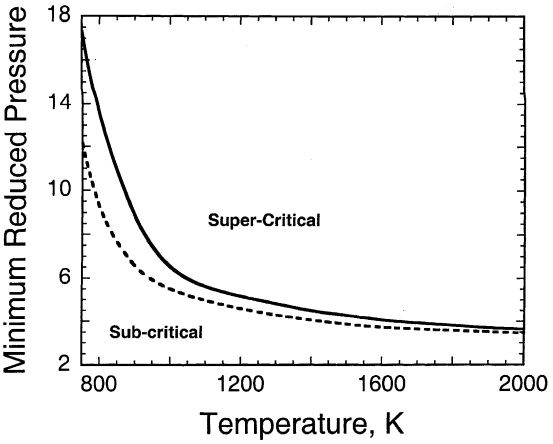

Fig. 7. Minimum reduced pressure at which the droplet surface reaches the critical mixing point versus temperature. The droplet diameter is 0.1 mm. Solid lines: diesel fuel. Dashed lines: single-component fuel.

stated above, contributes to the obvious volumetric dilation. Similarly, the smaller initial vaporization rate of the single-component fuel results in a slightly more obvious volumetric dilation, and the subsequent more rapid rise contributes to its larger surface regression rate, and hence a shorter lifetime, as shown in Fig. 3(a) and (b).

Fig. 6 shows the continuous change of the composition of the diesel fuel droplet versus time for the cases $P_r = 0.1$ and $P_r = 5$ of Fig. 3(a) and (b). The composition is expressed in terms of the mean molecular weight and the variance (the width of the composition distribution) of the liquid. The mean molecular weight of the vapor at the droplet surface is also presented for the same two pressure cases. As the vaporization process proceeds, the volatile (lighter) component continuously distills out, resulting in the continuous increase in mean molecular weight of both the liquid and the surface vapor. Both curves become closer and eventually reach the same values when the critical mixing point is reached at higher pressures. Correspondingly, the width of the liquid distribution decreases since the lighter end of the distribution shrinks. Comparing the results of both pressure cases, it can be seen that the rise rate of the liquid mean molecular weight and the decline rate of the liquid variance decrease with the increasing pressure, while the rise rate of the mean molecular weight of surface vapor increases with pressure. This indicates that the lighter species is relatively more difficult and the heavy species is easier to be distilled out for higher-pressure environments. This character has also been seen partly in VLE calculations as shown in Fig. 1(b).

Calculations were further conducted to determine the boundaries of the critical mixing state for both fuels. The results, which are presented in the form of the minimum reduced ambient pressure versus ambient temperature, are given in Fig. 7. In order to obtain the minimum pressure value, simulations were performed for increasingly higher pressures, but at fixed ambient temperature, until the critical mixing state was observed. Therefore, these curves actually represent the boundary between the sub-critical and super-critical vaporization states. Generally, the single-component substitute fuel reaches the critical mixing state earlier than the diesel fuel mixture does. The difference between them increases with decreasing environment temperature. Since the temperatures considered here approximately correspond to the temperature range mostly experienced in practical combustion devices, these results also emphasize the importance of considering the complex mixture nature of practical fuels in practical applications.

4. Summary and concluding remarks

A new comprehensive model for the transient high-pressure vaporization process of droplets of complex liquid mixtures with large numbers of components has been developed. The governing equations for both liquid- and gas-phase semi-continuous systems are derived that are applicable for any kind of distribution function. Formulae for the VLE of semi-continuous interface are derived that are general for any cubic type EOS. Correlations for calculating the properties of continuous species are also formulated.

The model is further applied to calculate the VLE and the transient sub- and super-critical vaporization processes for a typical petroleum fuel – diesel fuel. The results characterize the characteristics of the VLE and the droplet vaporization process of complex liquid mixture. The comparison with the corresponding results

of its single-component substitute fuel also emphasizes the importance of considering the multi-component nature of practical fuels.

This paper provides a new means for more realistically describing and treating the VLE and the high-pressure vaporization process of practical fuels. Further work will be focused on the consideration of more general distribution functions for other petroleum-derived fuels.

Acknowledgements

This work was supported by Caterpillar Inc. and the DOE/Sandia Laboratories.

Appendix A. Governing equations for semi-continuous phases in spherically symmetric system

The full set of governing equations in spherically symmetric system for both gas- and liquid-phase semi-continuous systems is derived in the following. The composition distribution function for the continuous species is assumed to be two-parameter type.

For gas-phase equations ($r > r_s$), based on Eq. (3) the governing equations for the continuity of fuel vapor are derived as:

$$\begin{aligned}&\frac{\partial}{\partial t}(\rho y_f)+\frac{1}{r^2}\frac{\partial}{\partial r}(\rho y_f u r^2)\\&\quad=\frac{1}{r^2}\frac{\partial}{\partial r}\left[\rho\overline{D}_m r^2\frac{\partial y_f}{\partial r}+y_f\frac{\partial}{\partial r}(\rho\overline{D}_m r^2)\right.\\&\qquad\left.-y_f\int_0^\infty f^v(\tau)\frac{\partial}{\partial r}(\rho D_{\tau m}r^2)\,\mathrm{d}\tau\right],\end{aligned}\tag{A.1}$$

$$\begin{aligned}&\frac{\partial}{\partial t}(\rho y_f\theta)+\frac{1}{r^2}\frac{\partial}{\partial r}(\rho y_f\theta u r^2)\\&\quad=\frac{1}{r^2}\frac{\partial}{\partial r}\left[\rho\tilde{D}_m r^2\frac{\partial}{\partial r}(y_f\theta)+y_f\theta\frac{\partial}{\partial r}(\rho\tilde{D}_m r^2)\right.\\&\qquad\left.-y_f\int_0^\infty f^v(\tau)\tau\frac{\partial}{\partial r}(\rho D_{\tau m}r^2)\,\mathrm{d}\tau\right],\end{aligned}\tag{A.2}$$

$$\begin{aligned}&\frac{\partial}{\partial t}(\rho y_f\psi)+\frac{1}{r^2}\frac{\partial}{\partial r}(\rho y_f\psi u r^2)\\&\quad=\frac{1}{r^2}\frac{\partial}{\partial r}\left[\rho\hat{D}_m r^2\frac{\partial}{\partial r}(y_f\psi)+y_f\psi\frac{\partial}{\partial r}(\rho\hat{D}_m r^2)\right.\\&\qquad\left.-y_f\int_0^\infty f^v(\tau)\tau^2\frac{\partial}{\partial r}(\rho D_{\tau m}r^2)\,\mathrm{d}\tau\right],\end{aligned}\tag{A.3}$$

where r is the radial coordinate, θ and ψ are, respectively, the first and the second moments of the fuel vapor distribution function. $D_{\tau m}$ is the diffusion coefficient of the element with property τ in gas-phase mixture. Coefficients $\bar{D}, \tilde{D}$, and $\hat{D}$ are defined as:

$$\bar{D}_m=\int_0^\infty D_{\tau m}f^v(\tau)\,\mathrm{d}\tau,$$

$$\tilde{D}_m\theta=\int_0^\infty D_{\tau m}\tau f^v(\tau)\,\mathrm{d}\tau,$$

$$\hat{D}_m\psi=\int_0^\infty D_{\tau m}\tau^2 f^v(\tau)\,\mathrm{d}\tau$$

and will be given below. Since the spatial differential forms of the last two terms in Eqs. (A.1)–(A.3) are identical to each other, they are cancelled out in actual numerical calculation. For discrete species, the conventional continuity equation is applied:

$$\begin{aligned}&\frac{\partial\rho_s}{\partial t}+\frac{1}{r^2}\frac{\partial}{\partial r}(\rho_s u r^2)=\frac{1}{r^2}\frac{\partial}{\partial r}\left[\rho D_{sm}r^2\frac{\partial}{\partial r}\left(\frac{\rho_s}{\rho}\right)\right]\\&\quad(s=1,2,\ldots,N),\end{aligned}\tag{A.4}$$

where D_{sm} is the diffusion coefficient of sth discrete species in the gas-phase mixture.

The momentum and energy equations for the gas-phase mixture are:

$$\begin{aligned}&\frac{\partial\rho u}{\partial t}+\frac{1}{r^2}\frac{\partial}{\partial r}(\rho u^2 r^2)+\frac{\partial P}{\partial r}\\&\quad=\frac{1}{r^2}\frac{\partial}{\partial r}\left[2\mu r^2\frac{\partial u}{\partial r}+\lambda\frac{\partial}{\partial r}(ur^2)\right]\\&\qquad-\frac{2}{r^2}\left[2\mu u+\frac{\lambda}{r}\frac{\partial}{\partial r}(ur^2)\right],\end{aligned}\tag{A.5}$$

$$\begin{aligned}&\frac{\partial\rho I}{\partial t}+\frac{1}{r^2}\frac{\partial}{\partial r}(\rho I u r^2)+\frac{P}{r^2}\frac{\partial}{\partial r}(ur^2)\\&\quad=\frac{1}{r^2}\frac{\partial}{\partial r}\left\{r^2k\frac{\partial T}{\partial r}+\rho r^2\left[\sum_{s=1}^{N}D_{sm}h_s(T)\frac{\partial}{\partial r}\left(\frac{\rho_s}{\rho}\right)\right.\right.\\&\qquad\left.\left.+D_m^h\bar{h}(T)\frac{\partial y_f}{\partial r}\right]\right\}+\frac{\partial u}{\partial r}\left[2\mu\frac{\partial u}{\partial r}+\frac{\lambda}{r^2}\frac{\partial}{\partial r}(ur^2)\right]\\&\qquad+\frac{2u}{r^2}\left[2\mu u+\frac{\lambda}{r}(ur^2)\right],\end{aligned}\tag{A.6}$$

where μ and λ are the viscosity and the second viscosity coefficients of the gas-phase mixture, and

$$\bar{h}(T)=\int_0^\infty f^v(\tau)h(\tau,T)\,\mathrm{d}\tau,$$

$$D_m^h\bar{h}(T)=\int_0^\infty f^v(\tau)D_{\tau m}h(\tau,T)\,\mathrm{d}\tau$$

where $h(\tau,T)$ is obtained from the following formula:

$$h(\tau,T)=R[c_{p1}(T)+c_{p2}(T)\tau]T,$$

where:

$$c_{p1}=c_{10}+c_{11}T+c_{12}T^2+c_{13}T^3,$$

$$c_{p2}=c_{20}+c_{21}T+c_{22}T^2+c_{23}T^3.$$

The values of the constants are [13]:

$$c_{10} = 2.465, \qquad c_{11} = -1.144 \times 10^{-2},$$
$$c_{12} = 1.759 \times 10^{-5}, \qquad c_{13} = -5.972 \times 10^{-9},$$
$$c_{20} = -3.561 \times 10^{-2}, \qquad c_{21} = 9.367 \times 10^{-4},$$
$$c_{22} = -6.030 \times 10^{-7}, \qquad c_{23} = -1.324 \times 10^{-10}.$$

D_m^h is taken to be the same as $\bar{D}_m$ in this work.

For liquid-phase equations ($r < r_s$), based on Eq. (11) the governing equations for the liquid fuel phase are derived as:

$$(x_{\mathrm{feq}} - y_f)\dot{m} = c_l r_s \frac{v_a}{3}\frac{\mathrm{d}x_f}{\mathrm{d}t} - \left[\rho\bar{D}_m \frac{\partial y_f}{\partial r} + y_f \frac{\partial}{\partial r}(\rho\bar{D}_m) - y_f \int_0^\infty f^v(\tau)\frac{\partial}{\partial r}(\rho D_{\tau m})\,\mathrm{d}\tau\right]\Bigg|_{r_s^+}, \tag{A.7}$$

$$\frac{c_l r_s}{3} x_{\mathrm{feq}} \frac{\mathrm{d}\theta^l}{\mathrm{d}t} = \left[(x_{\mathrm{feq}}\theta^l - y_f\theta)\dot{m} - \frac{c_l r_s}{3} v_a \theta^l \frac{\mathrm{d}x_f}{\mathrm{d}t} + \rho\tilde{D}_m \frac{\partial}{\partial r}(y_f\theta) + y_f\theta\frac{\partial}{\partial r}(\rho\tilde{D}_m) - y_f \times \int_0^\infty f^v(\tau)\tau\frac{\partial}{\partial r}(\rho D_{\tau m})\,\mathrm{d}\tau\right]\Bigg|_{r_s^+}, \tag{A.8}$$

$$\frac{c_l r_s}{3} x_{\mathrm{feq}} \frac{\mathrm{d}\psi^l}{\mathrm{d}t} = \left[(x_{\mathrm{feq}}\psi^l - y_f\psi)\dot{m} - \frac{c_l r_s}{3} v_a \psi^l \frac{\mathrm{d}x_f}{\mathrm{d}t} + \rho\hat{D}_m \frac{\partial}{\partial r}(y_f\psi) + y_f\psi\frac{\partial}{\partial r}(\rho\hat{D}_m) - y_f \int_0^\infty f^v(\tau)\tau^2\frac{\partial}{\partial r}(\rho D_{\tau m})\,\mathrm{d}\tau\right]\Bigg|_{r_s^+}, \tag{A.9}$$

where θ^l and ψ^l are, respectively, the first and the second moments of the distribution function for the liquid fuel. Again, the last two terms in Eqs. (A.7)–(A.9) are cancelled out due to the equal differential forms.

The critical properties of the continuous species are calculated using Eq. (19) for the critical temperature and pressure, and the following formula for the critical volume [11]:

$$V_c = a_v + b_v\tau, \tag{A.10}$$

where $a_v = 15.903\ \mathrm{cm^3/mol}$ and $b_v = 4.103\ \mathrm{cm^3/mol^2}$. The comparison between the predicted results using these formulae and the data of [14] is presented in Fig. 8. It is seen that the predictions match the data very well. With these formulae for predicting the critical properties, the viscosity and the thermal conductivity of the continuous species are then calculated with the same formulae as those for the discrete species. For diffusion-related coefficients, the following formulae were employed for the low-pressure calculation [10]:

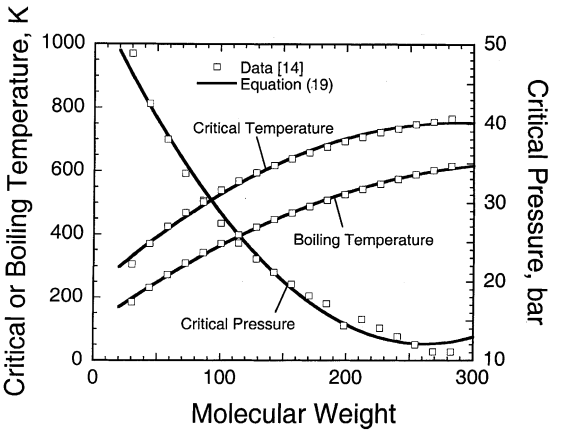

Fig. 8. Comparison of predictions of Eq. (19) for the critical and boiling properties of *n*-alkanes with the data of [14].

$$\bar{D}_m = (a_\mathrm{D} + b_\mathrm{D}\theta)\phi_\mathrm{D},$$
$$\tilde{D}_m = \left(a_\mathrm{D} + b_\mathrm{D}\frac{\psi}{\theta}\right)\phi_\mathrm{D}, \tag{A.11}$$
$$\hat{D}_m = \left[a_\mathrm{D} + \frac{b_\mathrm{D}}{\psi}(\gamma_\mathrm{s}\sigma^3 + 3\theta\sigma^2 + \theta^3)\right]\phi_\mathrm{D},$$

where γ_s is the skewness coefficient of the distribution, which for a Γ distribution function is given by $\gamma_\mathrm{s} = 2/\sqrt{2}$. The temperature dependence $\phi_\mathrm{D} = T^{5/2}/(T + 250)$. The constants $a_\mathrm{D} = 2.89 \times 10^{-9}$ and $b_\mathrm{D} = -6.60 \times 10^{-12}$. The units of these coefficients are $\mathrm{m^2/s}$. High-pressure effects were considered for these coefficients by using the Takahashi correlation [14].

Appendix B. Equation of state for semi-continuous mixtures

To describe the states of semi-continuous mixtures of gas and liquid phases and perform VLE calculations, an equation is needed to describe the P–V–T properties of these systems. The cubic type Eq. (7) is applied to semi-continuous mixtures via mixing rules for parameters a and b. For a system with N discrete species and M family of continuous fractions, we obtain for the gas-phase via mixing rule [20]:

$$b = \sum_{i=1}^{N} y_i b(i) + \sum_{m=1}^{M} (y_f)_m \int_\tau f_m^v(\tau) b(\tau)\,\mathrm{d}\tau, \tag{B.1}$$

$$a = \sum_{i=1}^{N}\sum_{j=1}^{N} y_i y_j a(i,j) + 2\sum_{i=1}^{N}\sum_{m=1}^{M} y_i (y_f)_m \times \int_\tau f_m^v(\tau) a(i,\tau)\,\mathrm{d}\tau + \sum_{m=1}^{M}\sum_{n=1}^{M}(y_f)_m (y_f)_n \times \int_\tau \int_{\tau^+} f_m^v(\tau) f_n^v(\tau^+) a(\tau,\tau^+)\,\mathrm{d}\tau\,\mathrm{d}\tau^+, \tag{B.2}$$

Table 3
Expressions for parameters a and b for two cubic EOS [14]

Equation	b	a
Peng–Robinson (PR)	$\frac{0.07780RT_c}{P_c}$	$\frac{0.45724R^2T_c^2}{P_c}[1+f_\omega(1-T_r^{0.5})]^2$
		$f_\omega = 0.37464 + 1.54226\omega - 0.26992\omega^2$
Soave–Redlich–Kwong (SRK)	$\frac{0.08664RT_c}{P_c}$	$\frac{0.42748R^2T_c^2}{P_c}[1+f_\omega(1-T_r^{0.5})]^2$
		$f_\omega = 0.480 + 1.574\omega - 0.176\omega^2$

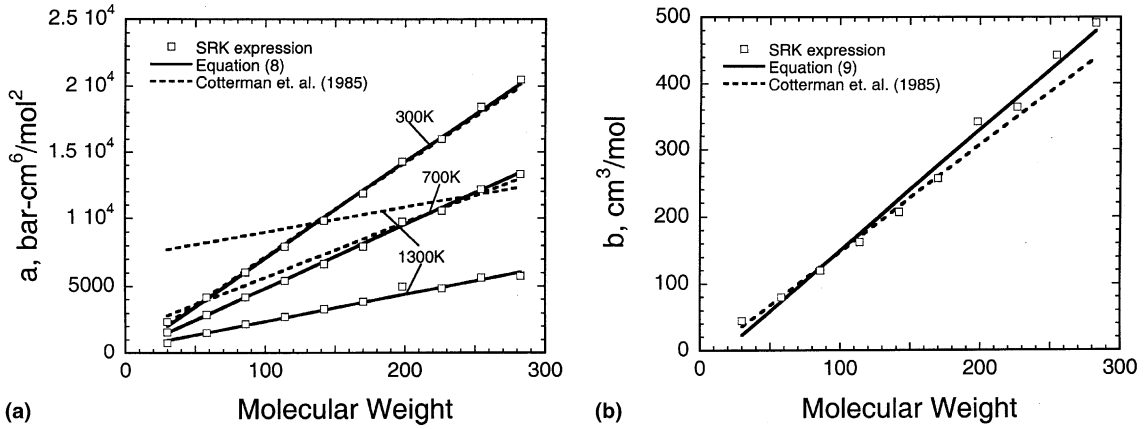

Fig. 9. Comparison for (a) parameter a of n-alkanes among the results of SRK-EOS expression, Eq. (8), and those of Cotterman et al. formulae [20] and (b) parameter b of n-alkanes among the results of SRK-EOS expression, Eq. (9), and those of Cotterman et al. formulae [20].

where y_i and $(y_f)_m$ are the gas-phase mole fractions for the ith discrete species and the mth family of continuous species, respectively. Similar relations hold for the liquid-phase.

Expressions for a and b for each discrete species are shown in Table 3. For continuous fractions, they are given by Eqs. (8) and (9). Figs. 9(a) and (b) present comparisons for parameters a and b of n-alkanes, respectively, among the calculated results using Eqs. (8) and (9), those calculated using Cotterman et al. formulae [20], and the data obtained using SRK-EOS expressions (see Table 3). As seen in the figures, Eqs. (8) and (9) reproduce SRK-EOS expressions very well for all temperature cases, while Cotterman et al. formulae are unacceptable for high-temperature conditions.

The cross terms in the mixing rules are given by a geometric mean corrected with a binary interaction coefficient, k:

$$\begin{aligned} a(i,j) &= a^{0.5}(i,i)a^{0.5}(j,j)(1-k_{ij}),\\ a(i,\tau) &= a^{0.5}(i,i)a^{0.5}(\tau,\tau)(1-k_{i\tau}),\\ a(\tau,\tau^+) &= a^{0.5}(\tau,\tau)a^{0.5}(\tau^+,\tau^+)(1-k_{\tau\tau^+}). \end{aligned} \tag{B.3}$$

For the discrete–discrete cross term, interaction coefficient k_{ij} is set to a constant value. For the discrete–continuous or continuous–continuous cross term, $k_{i\tau}$ or $k_{\tau\tau+}$ may be expressed as a function of molecular weight. Since there are no data available for diesel fuel–nitrogen system yet, these are taken to be zero in this work.

References

[1] W.A. Sirignano, C.K. Law, Transient heating and liquid-phase mass diffusion in fuel droplet vaporization, Adv. Chem. Ser. 166 (1978) 3–26.
[2] S.D. Givler, J. Abraham, Supercritical droplet vaporization and combustion studies, Prog. Energy Combust. Sci. 22 (1996) 1–28.
[3] J. Stengele, H.J. Bauer, S. Wittig, Numerical study of bicomponent droplet vaporization in a high-pressure environment, ASME Paper 96-GT-442, 1996.
[4] E.W. Curtis, A. Uludogan, R.D. Reitz, A new high pressure droplet vaporization model for diesel engine modeling, SAE 952431, 1995.
[5] G.-S. Zhu, S.K. Aggarwal, Fuel droplet vaporization in a supercritical environment, ASME Paper 99-GT-301, 1999.

[6] G.-S. Zhu, S.K. Aggarwal, Transient supercritical droplet vaporization with emphasis on the effects of equation of state, Int. J. Heat Mass Transfer 43 (2000) 1157–1171.
[7] J. Abraham, S.D. Givler, Conditions in which vaporizing fuel drops reaching a critical state in a diesel engine, SAE Paper 990511, 1999.
[8] R.S. Lazar, G.M. Faeth, Bipropellant droplet combustion in the vicinity of the critical point, in: Proceedings of the 13th International Symposium on Combustion, Combustion Institute, 1971, pp. 801–811.
[9] K.C. Hsieh, J.S. Shuen, V. Yang, Droplet vaporization in high-pressure environments, I: near critical conditions, Combust. Sci. Technol. 76 (1991) 111–132.
[10] J. Tamim, W.L.H. Hallett, Continuous thermodynamics model for multi-component vaporization, Chem. Eng. Sci. 50 (18) (1995) 2933–2942.
[11] A.M. Lippert, R.D. Reitz, Modeling of multi-component fuels using continuous distributions with application to droplet evaporation and sprays, SAE 972882, 1997.
[12] B. Gal-Or, H.T.J.R. Cullinan Jr., R. Galli, New thermodynamic transport theory for systems with continuous component density distributions, Chem. Eng. Sci. 30 (1975) 1085–1092.
[13] G.F. Chou, J.M. Prausnitz, Adiabatic flash calculations for continuous or semicontinuous mixtures using an equation of state, Fluid Phase Equilibria 30 (1986) 75–82.
[14] R.C. Reid, J.M. Prausnitz, B.E. Poling, The Properties of Gases and Liquids, McGraw-Hill, New York, 1987.
[15] A.Y. Tong, W.A. Sirignano, Multicomponent droplet vaporization in a high temperature gas, Combust. Flame 66 (1986) 221–235.
[16] T.B. Gradinger, K. Boulouchos, A zero-dimensional model for spray droplet vaporization at high pressures and temperatures, Int. J. Heat Mass Transfer 41 (1998) 2947–2959.
[17] T.H. Chung, M. Ajlan, L.L. Lee, K.E. Starling, Generalized multi-parameter correlation for nonpolar and polar fluid transport properties, Ind. Eng. Chem. Res. 27 (1988) 671–679.
[18] I.L. Byung, G.K. Michael, A generalized thermodynamic correlation based on three-parameter corresponding states, J. AIChE 21 (1975) 510–527.
[19] H. Hiroyasu, T. Kadota, T. Senda, T. Imamoto, Evaporation of a single droplet at elevated pressure and temperatures: experimental study, Trans. J. Soc. Mech. Eng. 40 (1974) 3147–3161.
[20] R.L. Cotterman, R. Bender, J.M. Prausnltz, Phase equilibria for mixtures containing very many components – development and application of continuous thermodynamics for chemical process design, Ind. Eng. Chem. Process Des. Dev. 24 (1) (1985) 194–203.